

Improvement of tunnel compensated quantum well infrared detector

Chaohui Li¹, Jun Deng^{1, †}, Weiye Sun¹, Leilei He¹, Jianjun Li¹, Jun Han¹, and Yanli Shi²

¹Key Laboratory of Optoelectronics Technology, Faculty of Information Technology, Beijing University of Technology, Beijing 100124, China

²School of Physics & Astronomy, Yunnan University, Kunming 650091, China

Abstract: To reduce the difficulty of the epitaxy caused by multiple quantum well infrared photodetector (QWIP) with tunnel compensation structure, an improved structure is proposed. In the new structure, the superlattices are located between the tunnel junction and the barrier as the infrared absorption region, eliminating the effect of doping concentration on the well width in the original structure. Theoretical analysis and experimental verification of the new structure are carried out. The experimental sample is a two-cycle device, each cycle contains a tunnel junction, a superlattice infrared absorption region and a thick barrier. The photosurface of the detector is $200 \times 200 \mu\text{m}^2$ and the light is optically coupled by 45° oblique incidence. The results show that the optimal operating voltage of the sample is -1.1 V , the dark current is $2.99 \times 10^{-8} \text{ A}$, and the blackbody detectivity is $1.352 \times 10^8 \text{ cm}\cdot\text{Hz}^{1/2}\cdot\text{W}^{-1}$ at 77 K . Our experiments show that the new structure can work normally.

Key words: infrared detector; tunnel compensation; superlattice

Citation: C H Li, J Deng, W Y Sun, L L He, J J Li, J Han, and Y L Shi, Improvement of tunnel compensated quantum well infrared detector[J]. *J. Semicond.*, 2019, 40(12), 122902. <http://doi.org/10.1088/1674-4926/40/12/122902>

1. Introduction

Traditional QWIPs based on intersubband transition have the advantages of good uniformity and high reliability^[1-3], which means they are suitable for fabricating large-scale focal plane arrays^[4]. Meanwhile, they are easy to fabricate into two or more color detectors^[5-7]. However, the principle of the QWIPs determines that the photocurrent of the devices is basically independent of the number of quantum wells^[8], which limits the performance of these detectors^[9]. To solve this problem, researchers have proposed a variety of improved structures^[10-13]. Among them, an improved quantum well infrared photodetector based on tunnel compensation was proposed. Deng^[14] made experimental samples based on this principle and carried out detailed experimental verification. The structure can increase the photocurrent as the number of quantum wells increases but the doping concentration of the material cannot be accurately controlled, resulting in difficulty in fabrication. Based on this, an improved structure is proposed by inserting superlattices between tunnel junctions and barriers. The superlattices replace irregular quantum wells and become the infrared absorption region of the detector. The working mechanism of the new detector is described. An experimental sample is made and the results of spectral response, dark current, and blackbody response at 77 K are given. The experimental results are roughly in line with expectations, proving that the design is feasible.

2. The principle and design points of the new structure

The schematic diagram of the multi-quantum well infrared

detector with tunnel compensation structure^[14] is shown in Fig. 1. J_p is the net photocurrent, $h\nu$ represents the energy of the incident photon. The i-AlGaAs layer and the PN junction consisting of P^+ -AlGaAs and N^+ -GaAs form barriers on both sides. The intermediate undepleted N^+ -GaAs layer forms a potential well. The empty quantum states generated by carrier excitation are filled by tunneling electrons, which reduces the recombination of photoelectrons in the well region, thus, the photocurrent of the device increases as the number of wells increases.

The drawback of this structure is that the doping concentration of epitaxy needs to be strictly controlled. Undepleted N^+ -GaAs layer is limited by barrier and tunnel junction depletion layer, forming quantum well. Assuming the width of N^+ -GaAs is L , the width of the n-type depletion layer is L_n , the width of quantum well is L_w , then $L_w = L - L_n$. Fig. 2 shows the relationship between doping and depletion layer width. L_n represents the width of depletion layer in N region and L_p represents the width of depletion layer in P region. Obviously, the width of the depletion layer of the tunnel junction is greatly affected by doping concentration. The quantum well is connected to the depletion layer, so the width of quantum well is closely related to doping concentration. The decrease of doping concentration of the N^+ -GaAs layer will result in the decrease of well width. As can be seen from Fig. 3, the width of the well affects the position and number of sub-levels. Meanwhile, the intersubband transition determines the absorption wavelength of the detector ($\Delta E = hc/\lambda$, ΔE represents the energy required for the transition of electrons from the ground state level of the excited state level, h represents the Planck constant, c represents the speed of vacuum light, and λ represents the wavelength of response.). If there are two sub-levels in a quantum well, then the increase in the well's width will lead to an increase in the response wavelength. This means that the deviation from dop-

Correspondence to: J Deng, dengsu@sbjut.edu.cn

Received 26 FEBRUARY 2019; Revised 22 MAY 2019.

©2019 Chinese Institute of Electronics

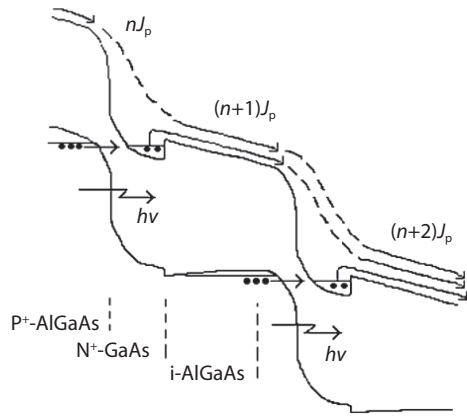


Fig. 1. Schematic diagram of the multi-quantum well infrared detector with tunnel compensation structure^[14] (under the reverse bias).

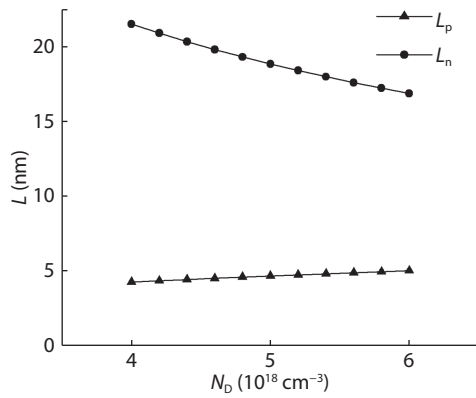


Fig. 2. The relationship between N_D and depletion layer width ($N_A = 2 \times 10^{19} \text{ cm}^{-3}$).

ing concentration may cause the fabricated devices to fail to meet the design requirements.

We proposed an improved structure to solve this problem. The working principle of the new infrared detector is presented in Fig. 4. As the picture shows, we inserted superlattices as the infrared absorption region after heavily doped PN junction, followed by a thick intrinsic barrier composed of i-AlGaAs. The tunnel compensated superlattice infrared detector separates depletion layers and quantum wells. The thickness of N^+ -GaAs layer in tunnel junction can be increased appropriately to prevent the expansion of the depletion layer. Compared with the original structure, the width of the quantum well is no longer influenced by the doping concentration of the tunnel junction. Thus, the sub-level of the quantum well can easily be controlled. This means that the effect of doping concentration error on device performance is reduced. In other words, the accuracy requirement of doping concentration is reduced. The difficulty of material growth is also reduced.

In an appropriate reverse bias, the ground state electrons of superlattices absorb photons jump to the excited state and across the barrier under the action of electric field. The photoelectrons are accelerated in the built-in potential field of the PN junction of the next cycle, passing through the next superlattice infrared absorption region at high speed. Meanwhile, the tunneling electrons from the p-GaAs valence band will fill into the empty quantum state of the ground state of the superlattices, reducing the recombination probability of photoelectrons.

Using a tunneling mechanism to fill empty quantum sta-

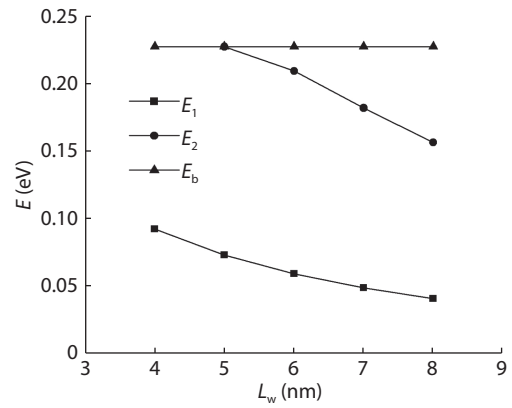


Fig. 3. The relationship between L_w and sub-levels. E_1 is the first level, E_2 is the second level and E_b is the barrier height.

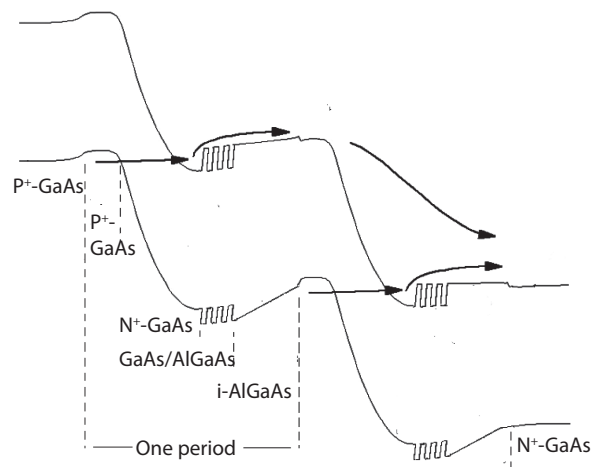


Fig. 4. Schematic diagram of the improved structure under the reverse bias.

tes can increase the photocurrent. This is a prerequisite for proper operation of the device. Therefore, the PN junction needs to be heavily doped to become a tunnel junction. The Fermi level in the n-region should be between the two subbands of the superlattices to ensure the injection efficiency of tunnel current into the ground state of superlattices. By measuring the peak voltage and the valley voltage of the tunnel junction, the Fermi level of the N region can be roughly estimated.

The superlattices are composed of wide and narrow band gap semiconductors that are periodically arranged. The barriers of superlattices need to be thin enough to form a tunneling resonance effect. Based on the tunneling resonance effect, the electrons traverse the barrier and fill the ground state of the superlattice. The position of the superlattice band is affected by the thickness of the well layer and the barrier layer. As soon as the structural parameters of the superlattice are determined, the absorption wavelength range of the device is determined. The transfer matrix method is a relatively simple and accurate method for calculating the position of subbands and the absorption wavelength.

The doping concentration of the superlattice should satisfy the condition that the electrons are sufficient to fill the ground state energy band and do not fill the excited state energy band. We designed the n-type doping concentration of the well to be $4 \times 10^{17} \text{ cm}^{-3}$ and the well width to be 6 nm. The calculated Fermi level^[15] of the superlattice is 6.4 meV

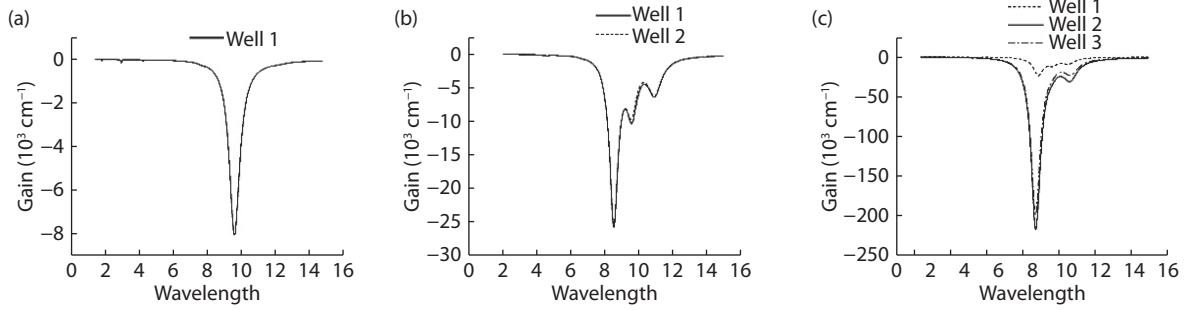


Fig. 5. The relationship between the gain and wavelength of different numbers of wells: (a) single well, (b) double well and (c) triple well.

Table 1. Structural parameters of the experimental sample.

		Material	Thickness (nm)
		P ⁺ -GaAs	300
2 cycles	20 cycles	P ⁺ -GaAs	12
		N ⁺ -GaAs	24
	i-Al _x Ga _{1-x} As $x = 0.28$	6	
	N ⁺ -GaAs	6	
	i-Al _x Ga _{1-x} As $x = 0.27$	40	
		N ⁺ -GaAs	500
Semi-insulating GaAs (100) substrate			

higher than the ground state level. Fig. 5 shows the relationship between the number of wells and the gain of the device. Our calculations show that the gain increases as the number of wells increases. Meanwhile, too many wells will lead to a great increase in the probability of photoelectron recombination. Under the action of the electric field ($> 10^7$ V/m) in the tunnel junction, the electron drift velocity will reach the maximum in a short time. The drift velocity then decreases gradually under the effect of scattering. With the relaxation time approximation and the relaxation time of 0.2 ps, the average free path of the electron is greater than 300 nm. We experimentally fabricated a structure of 20 quantum wells (the thickness is 240 nm) per cycle to ensure that the electrons can pass through a cycle.

3. Experiments and results

To verify the feasibility of the theory, we used MOCVD technology to grow an experimental sample. The sample has a photosensitive surface area of $200 \times 200 \mu\text{m}^2$ and is optically coupled by 45° oblique incidence. It is a two-period structure, where each period contains a tunnel junction, a superlattice region with multiple wells and a thick intrinsic barrier. The structural parameters of the sample are shown in Table 1.

The response spectrum of the sample tested by Fourier transformation infrared spectrometer (FTIR) at 77 K is shown in Fig. 6. The device has a peak response wavelength of $7.73 \mu\text{m}$. According to the transfer matrix method, the waveband that the device can absorb is about $7.48\text{--}8.93 \mu\text{m}$, which is basically consistent with the test result.

Fig. 7 shows the dark current characteristics of the sample at different temperature. One negative differential resistance region is shown in Fig. 7(a) at positive bias. The position of the peak and the valley of the negative differential resistance region is 4.2 and 4.35 V, respectively, at low temperature. This indicates that the Fermi level above the conduction band of N⁺-GaAs 150 meV, approximately, is between the ground state and the first excited state in the superlattice re-

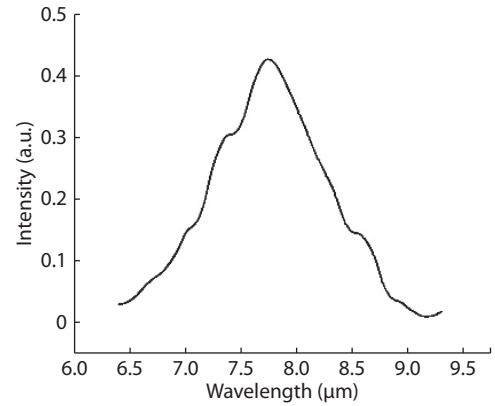


Fig. 6. Response spectrum of sample at 77 K.

gion. This means that the empty quantum states generated by infrared radiation in ground state will be refilled by inter-band tunneling process. The reverse I - V curve is shown in Fig. 7(b). A small leakage current can be obtained when the reverse bias voltage is less than 1.1 V at 77 K. This is due to the unification of Fermi levels at zero bias, the close valence band of P⁺-GaAs, the conduction band of N⁺-GaAs, and the existence of large barriers in the device. To ensure the current transport, a large enough bias voltage must be applied to flatten the barrier. At this time, the photocurrent of the device can cross the barrier and the dark current is small enough. For a dual-period device sample, only one barrier needs to be flattened, so the optimal operating voltage of the device is 1.1 V.

Fig. 8 shows the black body response test results of the device at 77 K. The blackbody temperature is 500 K. R represents the signal and N represents the noise. The maximum ratio of signal and noise is obtained when the reverse bias voltage is about 1.1 V. Simultaneously, the dark current is 2.99×10^{-8} A and the 500 K blackbody detectivity is $1.352 \times 10^8 \text{ cm}\cdot\text{Hz}^{1/2}\cdot\text{W}^{-1}$. As voltage V_b continues to increase, the dark current of the device grows rapidly. This happens because the ground state electrons are more likely to tunnel through the barrier under large bias voltage. The experimental results of the original structure can be referred to Refs. [14, 16]. By comparison, it can be seen that the results of the two structures are similar.

4. Conclusions

Based on the tunnel compensation multi-quantum well infrared detector, the superlattice layers are used as the infrared absorption region of the detector and the tunnel junctions provide tunnel compensation current for the superlat-

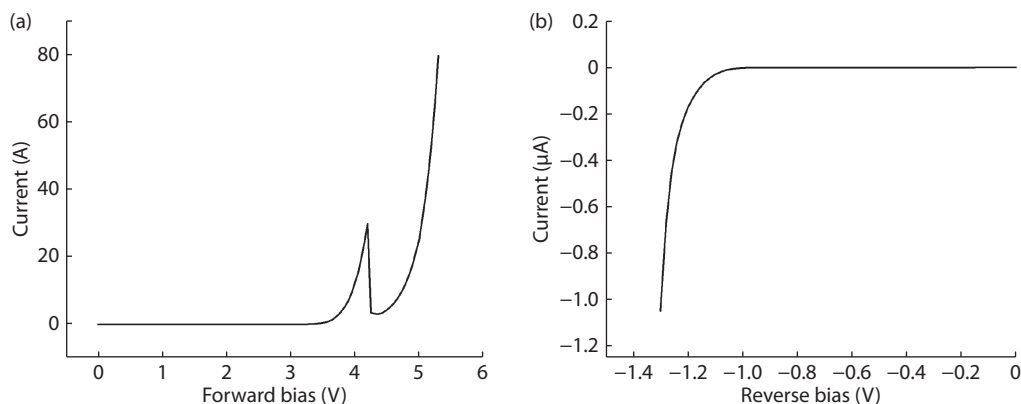


Fig. 7. Dark current versus applied bias of sample at 77 K. (a) Forward bias. (b) Reverse bias.

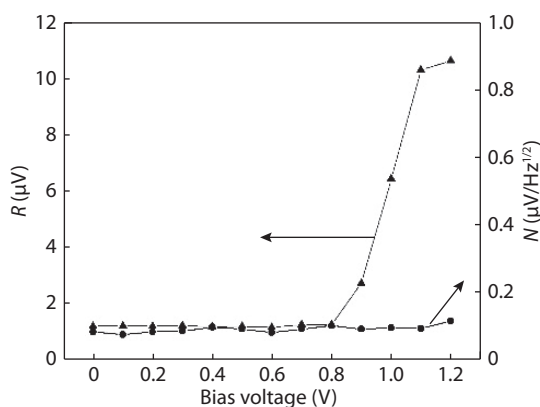


Fig. 8. Blackbody response test of sample at 77 K.

tices, which are easy to fabricate by MOCVD technology. Experimental samples of two-period structure were fabricated using GaAs and AlGaAs materials, and the response spectrum, dark current characteristics and blackbody response of the device are obtained. The results show that the optimal operating voltage of the sample is 1.1 V, the dark current is 2.99×10^{-8} A, and the blackbody detectivity is 1.352×10^8 cm \cdot Hz $^{1/2}\cdot$ W $^{-1}$ at 77 K. Owing to time constraints, detectors with more cycles have not been manufactured. In theory, however, detectors with more cycles can be expected to have larger photocurrents. The structural parameters of the device are subject to further optimization.

Acknowledgements

This work is supported by Beijing Natural Science Foundation (No. 4182011), the Development Foundation for Optoelectronics Technology Lab, Ministry of Education (No. PXM 2018_014204_500020), and National Natural Science Foundation of China (No. 61751502).

References

[1] Rogalski A. Recent progress in infrared detector technologies. *In-*

- frared Phys Technol*, 2011, 54, 136
- [2] Kataria H, Asplund C, Lindberg A, et al. Novel high-resolution VGA QWIP detector. *Proc SPIE*, 2017, 10177
- [3] Roodenko K, Choi K K, Clark K P, et al. Control over the optical and electronic performance of GaAs/AlGaAs QWIPs grown by production MBE. *Infrared Phys Technol*, 2017, 84, 33
- [4] Jhabvala M, Choi K K, Monroy C, et al. Development of a 1 K \times 1 K 8–12 μ m QWIP array. *Infrared Phys Technol*, 2007, 50, 234
- [5] Kaya Y, Ravikumar A, Chen G P, et al. Two-band ZnCdSe/ZnCd-MgSe quantum well infrared photodetector. *AIP Adv*, 2018, 8, 075105
- [6] Li Z F, Jing Y L, Zhou Y W. Multi-band integrated quantum well infrared photodetectors. *International Conference on Infrared Millimeter and Terahertz Waves*, 2018
- [7] Wu Y, Liu H M, Li P Z. Dual-band quantum well infrared photodetector with metallic structure. *Proc SPIE*, 2018, 10697
- [8] Rogalski A. Infrared detectors: an overview. *Infrared Phys Technol*, 2002, 43, 187
- [9] Haran T L, James J C, Lane S E, et al. Quantum efficiency and spatial noise tradeoffs for III–V focal plane arrays. *Infrared Phys Technol*, 2019, 97, 309
- [10] Eker S U, Hostut M, Ergun Y, et al. A new approach to quantum well infrared photodetectors: Staircase-like quantum well and barriers. *Infrared Phys Technol*, 2006, 48, 101
- [11] Choi K K, Allen S C, Sun J G, et al. Small pitch resonator-QWIP detectors and arrays. *Infrared Phys Technol*, 2018, 94, 118
- [12] DeCuir E A Jr, Choi K K, Sun J, et al. Progress in resonator quantum well infrared photodetector (R-QWIP) focal plane arrays. *Infrared Phys Technol*, 2015, 70, 138
- [13] Su G X, Liu L, Zang W B, et al. Highly efficient dielectric optical coupler for quantum well infrared photodetectors. *IEEE Photonics Technol Lett*, 2018, 30, 1167
- [14] Deng J, Shen G D, Lian P, et al. Optoelectronic transport mechanism from subband infrared absorption and tunneling regeneration. *Curr Appl Phys*, 2002, 2, 373
- [15] Billaha A, Das M K. Influence of doping on the performance of GaAs/AlGaAs QWIP for long wavelength applications. *Opto-Electron Rev*, 2016, 24(1), 25
- [16] Deng J. Study on novel GaAs/AlGaAs multi-quantum wells infrared photodetecting mechanism and MOCVD epitaxy technology. Beijing: Beijing University of Technology, 2005, 79